Building and Environment 245 (2023) 110864

Contents lists available at ScienceDirect

Building and Environment

journal homepage: www.elsevier.com/locate/buildenv

Sustainability to wind actions of a new roofing structure in a green university campus

Luisa Pagnini [a,*], Federico Delfino [b], Giuseppe Piccardo [a], Maria Pia Repetto [a]

[a] Department of Civil, Chemical and Environmental Engineering (DICCA), University of Genoa, Genoa, Italy
[b] Department of Electrical, Electronics and Telecommunication Engineering and Naval Architecture (DITEN), University of Genoa, Genoa, Italy

ARTICLE INFO

Keywords:
Environmental impact
Pedestrian wind comfort
Sustainability
Vaulted canopy roofs
Vegetation
Wind actions
Wind-tunnel tests

ABSTRACT

Wind actions and their impact on a sports field roof and its surroundings are extensively explored using wind tunnel tests and microclimate investigations based on accurate wind speed recordings, with a specific focus on the influence of the built environment and vegetation. The experimental analyses conducted on a scale model of the roofing structure yield appropriate coefficients that enhance the precision of estimating wind-induced pressures. These coefficients aid in optimizing the structure and ensuring its safety, effectively preventing overdesign while identifying areas of high peak pressure on the roof. Comparisons with regulatory guidelines and literature examples regarding the roof in isolation emphasize the significance of conducting a comprehensive analysis that considers the influence of surroundings for sustainability. Furthermore, transfer coefficients of the flow velocity are derived from the experimental analysis to translate the wind climate in the area to the pedestrian level. Pedestrian comfort analyses are performed using conventional methods, as well as considering the actual hourly variation of wind speed and daily activities within the university campus. This analysis encompasses the influence of vegetation and explores potential mitigation strategies, offering a fresh perspective to assess the liveability of the area, particularly suitable for specific social spaces such as university campuses.

1. Introduction

Urbanization is an essential component of a country's economic and social development, contributing to positive outcomes for its citizens when implemented in accordance with sustainable growth principles, minimizing environmental impact, enhancing social well-being, and ensuring the safety of residents.

Reducing the environmental impact of built-up areas by optimizing the use of structural materials is a key strategy to reduce embodied carbon emissions (e.g. Refs. [1,2]). Tree-planting initiatives play a vital role in climate and air quality regulation [3,4], as well as in mitigating natural disasters and wind effects on low-rise buildings [5]. Health and wellbeing are fundamental objectives of sustainability to be pursued by a balanced and responsible human-nature relationship, considering psychological well-being, and physical wellness as key priorities [6]. The integration of sustainability and safety is evident as both aim to preserve environmental and human resources.

Wind actions and effects on buildings and surrounding areas are strictly tied to the windiness at the site and to the shape of same buildings and environment. Codes and standards supply reference values of the basic wind, and suitable transformation laws for transferring the wind velocity to the site of interest. Pressure coefficients are also available for commonly shaped structures usually deriving from experimental tests on models in isolation. However, slight change of morphology as well as aerodynamic interactions within the built environment may lead to a significant variation in wind loads (e.g. Ref. [7]). Relying on conservative values to compensate for the lack of specific information may be uncertain and does not guarantee safety. It can also lead to overestimations of wind actions, resulting in higher construction costs, material waste, and conflicting sustainability principles. Additionally, buildings significantly impact microclimatic conditions through their location, orientation, design, material form, colors. These effects manifest as elevated temperatures, humidity, rainfall, air pressure, energy usage, wind speeds or poor ventilation [8]. While pedestrian outdoor thermal comfort has gained importance in designing sustainable cities (e.g. Refs. [9,10]), wind comfort and safety assessment typically focus on the mechanical effects of wind on people (e.g. Refs. [11,12]). City authorities recognize the significance of pedestrian wind comfort and safety, necessitating specific studies before approving new building projects or urban areas. For instance, City of London [13] has

* Corresponding author.
E-mail address: luisa.pagnini@unige.it (L. Pagnini).

https://doi.org/10.1016/j.buildenv.2023.110864
Received 30 June 2023; Received in revised form 13 September 2023; Accepted 20 September 2023
Available online 22 September 2023

drawn up a document providing general guidelines for wind microclimate assessment that is required as part of the planning applications of new development proposals.

Accurate studies of wind comfort and actions on structures can be pursued by combining statistical meteorological records with aerodynamic information that can be obtained by either wind tunnel modelling or Computational Fluid Dynamics (CFD) techniques (e.g. Refs. [14–16]), with strengths and limitations for both procedures [17, 18]. Nowadays, both physical and CFD techniques are often used in parallel to exploit their strengths and minimize their limitations ([19, 20]).

Urban vegetation, including green walls, parks, and tree planting, provides an effective solution to mitigate air temperature, pollutant diffusion, wind actions, and windiness at the pedestrian level. The use of "green" in the cities, including green walls, parks and tree planting, is a well-established mitigation strategy, which affects urban microclimate and pedestrian comfort through several processes among which evapotranspiration, shading, interaction with air movement and visual perception [21–23]. The effects of trees on pedestrian comfort and health have been examined mainly from a numerical point of view, in some cases validated through experimental results from wind tunnel and field campaigns (e.g. Refs. [24–26]). On the other hand, the presence of urban green infrastructures, which include site-scale vegetation and building-integrated vegetation, influences the energy consumption [27], microclimate [28] and wind actions on low-rise buildings. Given the heterogeneity of urban vegetation, there is not a systematic knowledge about the impact of trees on the well-being of citizens and about the effects at local scale of changing the density and typology of trees. Furthermore, there is no technical standardization regarding the type of trees used and the mitigation effects of predefined arrangements, especially with reference to scale tests in wind tunnel.

This paper showcases the outcomes of a wind tunnel campaign conducted to examine the influence of the surrounding environment on the wind pressure experienced by a sports field roof in a university campus, as well as its impact on pedestrian comfort within the area. Concerning wind pressure measurements on the canopy, the impact of the surrounding environment, including neighbouring buildings, and topography are compared with the specific findings previously presented in Ref. [29] for the isolated structure. The assessment of the pedestrian comfort is conducted in presence of vegetation by employing classical procedures tailored to address the specific usage of the area and the activities of the dwellers within the site. The obtained results enable the examination of the sustainability aspects of the newly constructed area, focusing on optimizing the structural material to ensure both structural safety and the overall liveability of the built-up environment.

Section 2 presents an overview of the Savona Campus of the University of Genova as a sustainable district model for local society and institutions. It describes the proposed new vaulted roof and provide insights into the wind climate characteristics in the area. In Section 3 the scale model of the vaulted canopy roof and the wind tunnel setup are described. Section 4 introduces the analysis methodology employed in this paper to evaluate wind pressures on the roofing structure and assess pedestrian comfort in the newly built area. Section 5 outlines main results in terms of net mean and peak pressure coefficients with and without the influence of surroundings, as well as transfer coefficients to quantify wind effects at the pedestrian level. An extensive discussion of the experimental results is presented in Section 6, incorporating comparisons with values derived from codes to optimize structural sizing and ensure safety. The map illustrating pedestrian comfort is discussed, focusing on the mitigation provided by the environment and vegetation. Furthermore, the variations in windiness throughout the day are considered in relation to the activities taking place on the campus. Section 7 summarizes the key conclusions drawn from this study.

2. The roofing structure at the Savona Campus of the Genoa University and its local wind climate

2.1. The Savona Campus

The Savona Campus of the Genoa University is a medium-small campus located in the coastal city of Savona populated by more than 2000 students, university teachers, employees and company workers, offering catering services and student accommodations [30]. These and other social and cultural services, such as library, conference halls, green areas and sports facilities are also available to the population, making the campus a cultural reference point for citizens and enterprises, representing a reference prototype of smart city for the realization of pilot projects in the field of energy and sustainability. Innovative energy systems have been also realized for reducing operating costs and pollutant emissions embedded in an intelligent and sustainable microgrid that provides electricity and thermal energy from renewable sources (PV, solar plants, geothermal heat pumps), cogenerating micro-turbines, gas boilers, absorption chillers and electrochemical storage [31]. The campus represents therefore a "Living Lab" showing a real application of the smart city concept to population and external stakeholders.

Special attention is paid to the environment, sports and open-air activities open to the population, which are catalyst for healthy urban development that is attentive to the well-being of citizens [32]. Several infrastructures allow to train open-air sports as tennis and football, to practice a total-body training inside a smart gym (able to produce electricity from the human movement), or outdoors over an open-air fitness trail. A sport hub for sea and water activities is now proposed on the beach near the Campus as well as the retrofitting and roofing of the existing football field to create an indoor multi-purpose facility to train football, volleyball and basketball.

2.2. The sports field and the new roofing structure

The proposed roofing structure is made by arched steel trusses supported by steel and r.c. columns. Fig. 1 shows plan (a), section (b) and 3-D rendering (c) of the facility. Plan size is $B \times D = 32 \times 40$ m^2, the maximum height above the ground level is $H = 11.2$ m. The rise of the arch is quantifiable between $f = 6.7$ m and 8 m, with a rise/span ratio f/B between 0.2 and 0.25, given the different height of the eaves line for the two sides of the roof. It has a symmetry axis parallel to the smallest dimension which makes an angle of about 30° with the north direction. It is covered by a metal sheet over the entire vault up to about $h = 4.5$ m above the ground on the one side, and to about 3.2 m above the ground on the other side, bordering a small building used as dressing room. It has a skylight at top covered by metal sheet (i.e., it is not venting) which rises 0.3 m from the roof. A 2 m-high plexiglas barrier surrounds the playing field. Dashed lines in Fig. 1b reproduces a pitched roof with the same rise-to-span ratio that will be considered in the following for comparisons.

The structure is located in the central area of the campus (Fig. 2) surrounded by secular pines up to 30 m tall. On the South and East side there is a flat terrain accompanied by low-rise buildings, reaching approximately 8.5 m in height. To the West, the ground level gradually increases by a few meters. On the North side there is a slight relief on which stands the library, whose roof level (building height plus basement level) is higher than the canopy. In front of the sports field runs the main street that crosses the campus, roughly aligned along NW-SE direction.

2.3. Local wind climate

Wind speed was recorded from 2014 to 2018 by a sonic anemometer in the port of Savona (with a sampling frequency of 10 Hz), about 3 km far from the campus, in the framework of the European Project "Wind

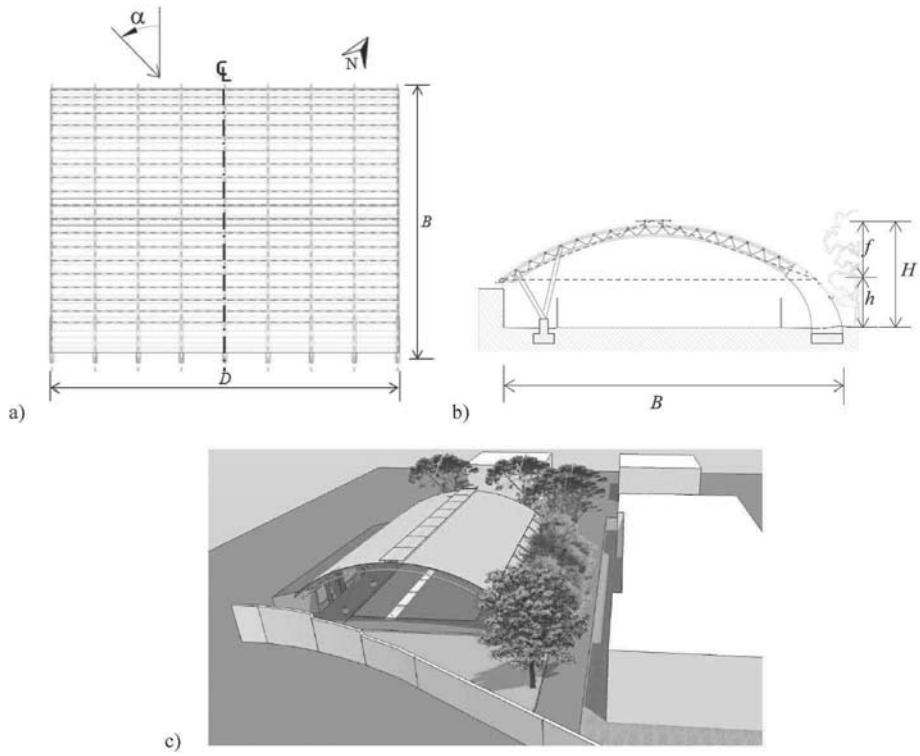

Fig. 1. Plan (a), vertical section (b) and 3-D rendering (c) of the proposed roofing structure.

Fig. 2. Savona campus area (the circle red highlights the sports field position). (For interpretation of the references to color in this figure legend, the reader is referred to the Web version of this article.)

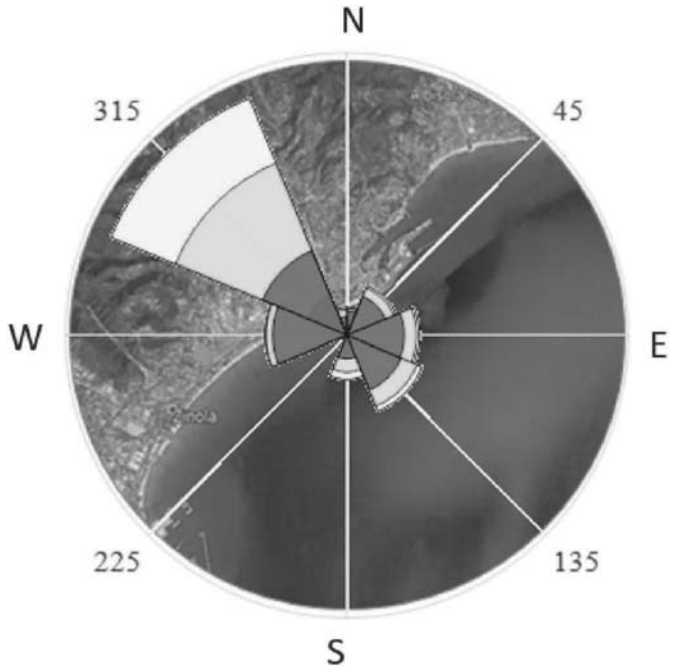

Fig. 3. Wind rose at the anemometer site.

and Ports" [33]. Fig. 3 shows the wind rose of the 10-min recorded mean wind speed superimposed to the Google map centered at the anemometer position. Wind direction refers to the North. The red dot indicates the site of the University campus where the sports field is located. The coastal line in the Figure separates two main directional sectors, from which winds blow driven by different mechanisms. Sea sectors are approximately from 30° to 235°, characterized by lower roughness and flat surface; elsewhere there are land sectors (approximately from 235° to 360° and from 0° to 45°), characterized by high roughness and complex orography behind the city of Savona.

Fig. 4 shows the probability histogram of the 10-min mean wind speed for the wind blowing from the land (Fig. 4a) and from the sea (Fig. 4b). Land sector wind highlights a bimodal distribution which has

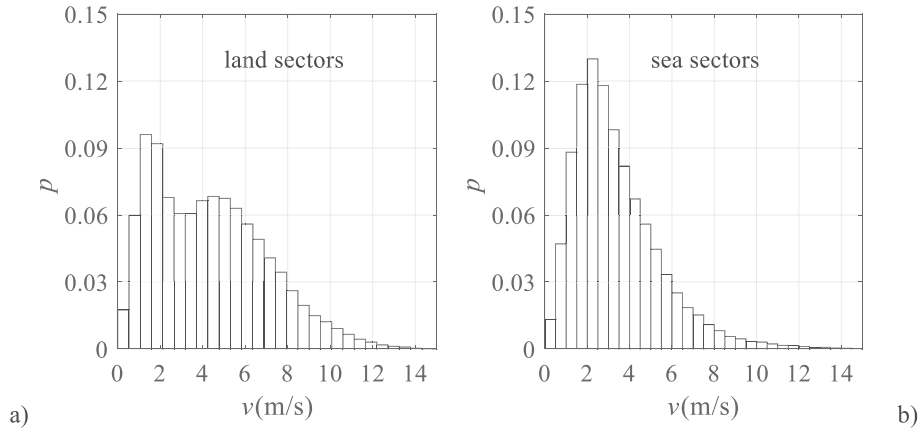

Fig. 4. Probability histograms for wind coming from the land (a) and from the sea (b).

been observed for heterogeneous wind regimes (e.g. Ref. [34]), while sea sector wind follows a typical Weibull distribution. Fig. 5 shows the hourly variation of the average wind speed. Wind blowing by the land (Fig. 5a) is averagely higher during day time, from about 9:00 a.m. to 6:00 p.m., especially in summer and spring season, suggesting the presence of two different generating physical mechanisms of land wind, at a global and at a local scale.

The mean wind velocity is 4.2 m/s. Prevailing wind direction is 300–330° at any time of the day, blowing from the mountains that surround the city of Savona [35]. It is noteworthy that this orientation aligns with the main street that traverses the Campus (see Fig. 2).

3. Scale model and wind tunnel setup of the roofing structure and its surroundings

The experimental tests were carried out at the "Giovanni Solari" atmospheric boundary layer wind tunnel of the University of Genoa. It is a closed-circuit type operating at atmospheric pressure; the working section is 8.8 m long, with a cross-section of 1.70 (width) × 1.35 (height) m.

The 1:100 scale model specifically designed for wind tunnel tests faithfully reproduces the sports field covering, its surroundings and vegetation (Fig. 6). The roof model is manufactured by a stereo-lithography 3D printer using transparent resin; it is about 3 mm thick to host printed ducts for pressure measurements; 166 pressure taps are located on the outer and the inner roof surfaces transmitting the signal within the roof thickness up to the longitudinal edges and then by flexible tubing, about 200 mm long, 0.8 mm in diameter, to multi-channel pressure scanners, having a measurement range of ±1 kPa

Fig. 6. Model on the turning table in the Giovanni Solari Wind Tunnel of the Genoa University.

and a sampling frequency of 650 Hz. Being the tubes short enough, no frequency corrections are needed to be applied to the measured data. Fig. 7 show the position of the pressure taps on the inner and outer side surfaces, respectively.

16 hot-wire omni-directional air velocity probes (Kanomax, visible in Fig. 8a) are placed in selected positions at the pedestrian level for environmental measurements, around the sports fields in the open space where people may walk or stand to watch sports matches (Fig. 8b, which also indicates the symmetry axis of the canopy with respect to the North and the main street that crosses the campus). The signals recorded by Kanomax probes are sampled at 10 Hz.

Measurements were conducted using three different setups. The first one reproduces buildings and surroundings, without replicating the

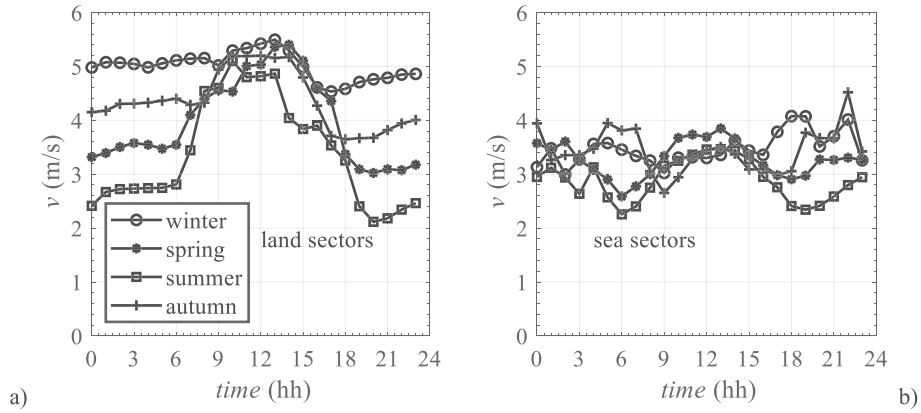

Fig. 5. Hourly wind velocity for wind coming from the land (a) and from the sea (b).

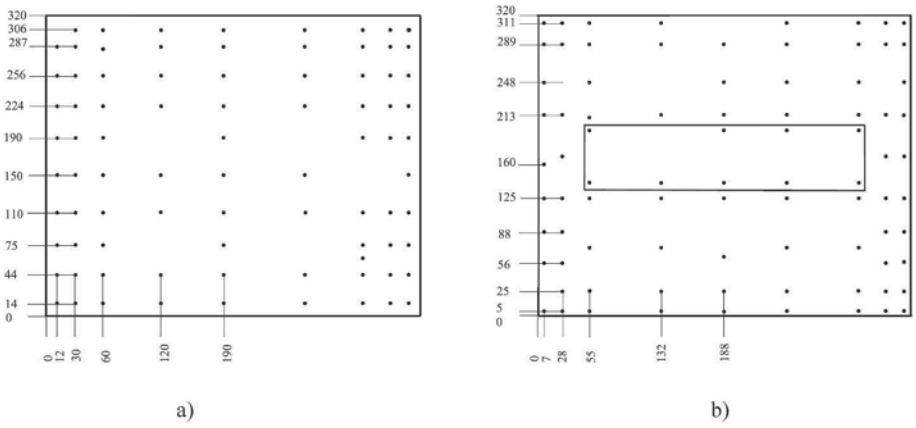

Fig. 7. Pressure taps on inner (a) and outer (b) surfaces; dimensions are in mm.

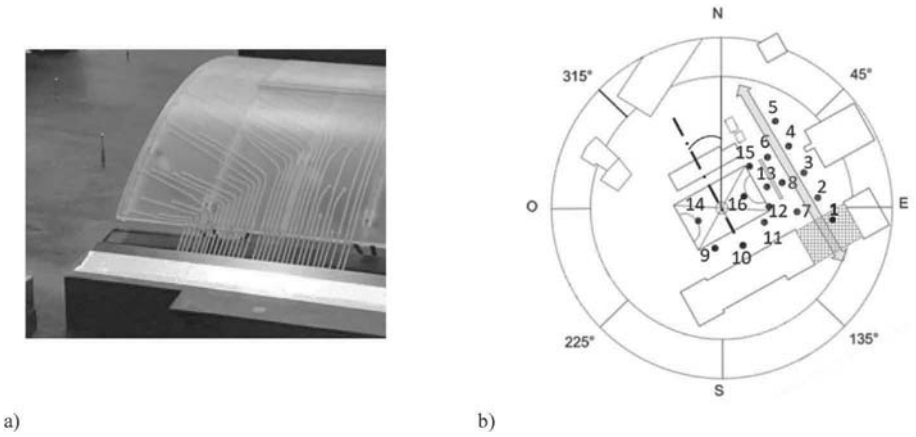

Fig. 8. Kanomax probe (a), investigated positions at the pedestrian level (b). The arrow in (b) indicates the pedestrian crossing road; the grey objects represent windbreak barrier and sunshade present in other configurations.

existing trees (Fig. 9a, setup 0). The second setup also reproduces the trees currently present around the sports field in the campus (setup 1, Fig. 9b). The third setup adds smaller trees than the existing ones, to evaluate possible improvement configurations (setup 2, Fig. 9c). Other configurations were also tested, with a sunshade and a windbreak barrier simulated by a porous copper sheet (Fig. 9d). The sunshade (that actually exists in the campus) covers the area between two buildings southeast of the canopy, above the pedestrian street that crosses the campus. The 2.2 cm high (2.2 m in full scale) windbreak barrier stands in front of the sports field. The positions of windbreakers and the pedestrian path are also reported in Fig. 8b. However, these configurations did not demonstrate any significant mitigation of the windiness at the

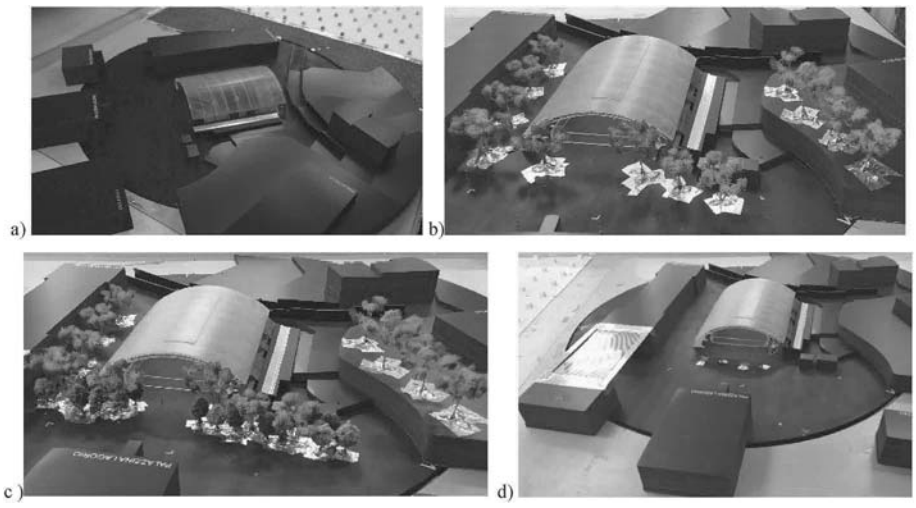

Fig. 9. Setup for pressure and pedestrian measurements without vegetation (setup 0, a), and for pedestrian measurements with actual trees (setup 1, b), with more trees (setup 2, c), with windbreakers and barriers (d).

pedestrian level and, then, the corresponding results were not included in the following.

Free stream pressure was measured by a Pitot static tube positioned upstream of the test section through a differential pressure gauge with a range of 0–5 in WC. The value of the air density used to convert the kinetic pressure into speed values is derived on the basis of the air temperature measured in the test chamber. A multi-hole probe ("TFI Cobra" probe) measures the three components of flow velocity at the height of 20 cm with respect to the ground level (20 m in real scale) for ambient measurements. It is positioned in the wind tunnel through a 3 degree-of-freedom robotic arm and supplies speed measurements inside a cone with an opening of ±45°. All these signals are recorded and sampled at 2 kHz.

Based on roughness maps built in the framework of the European Project "Wind and Ports" [33], using the cartography of land use and land cover of the Liguria Region, the roughness coefficient z_0 is assumed equal to 0.3 m for all wind sectors at the Campus site. The mean velocity $\overline{v}$, the longitudinal turbulence intensity I_u logarithmic profiles and the turbulence spectrum simulated in the wind tunnel are shown in Fig. 10a, b,c respectively, and compared with values target values supplied by CNR guidelines [36] for suburban area; $\overline{v}_{10}$ is the reference value of $\overline{v}$ measured at height 10 cm (10 m in full-scale conditions), that corresponds to a representative level of the roofing structure under investigation. The wind-tunnel $\overline{v}$ and I_u have been calculated using the local velocity measured at the corresponding height. The wind tunnel turbulence spectrum is obtained from the record of the undisturbed flow at the reference level $z = 10$ cm; the integral length scale L_u is estimated by fitting the spectrum with the Von Karman model, $L_u = 290$ mm (29 m in full scale). Wind speed is reasonably well-replicated, although there is some deviation in the integral scale, which tends to be smaller than the target value ($L_u = 48$ m) as is common for models of similar geometric scales (e.g. Ref. [37]). In this regard, Tieleman [38] argues that the integral length scale is not the primary factor affecting the peak pressure coefficient on low-rise buildings. However, the high-frequency range of the spectrum needs to be matched in the wind tunnel modelling to accurately simulate flow separation and reattachment. In any case, it is expected that the mean pressure coefficients are minimally affected by a similar difference in the turbulence integral length scale assessment. The blockage is less than 4%.

4. Analysis methodology

To investigate the impact of the environment on the wind behavior of the canopy and the overall liveability of the area, two distinct test campaigns were conducted. The first test campaign focused on measuring wind pressures on the roof in its actual context, including the topography and surrounding buildings. Vegetation was not reproduced at this stage of the research, as its temporary and changeable nature commonly leads to neglect the influence of trees on wind-induced pressures on structures. The results of this campaign can be compared to the outcomes of previous tests on the roofing in a flat environment, in order to evaluate the effect of surrounding.

The second test campaign concerned the measurement of wind speeds at the pedestrian level in the surrounding area. In this case the three set-ups previously described (Fig. 9) have been considered to investigate the role of vegetation on the liveability of the area.

Pressures on the outer and inner roof surfaces were simultaneously sampled at a frequency of 650 Hz for a duration of 180 s, equivalent to 120 min under full-scale conditions. After a thorough verification process to establish the ambient pressure as the reference static value [29], the model was investigated at 15° intervals in the counterclockwise wind direction, denoted by α. The measurements were conducted with respect to the symmetry axis, which aligns parallel to the shorter side B of the roofing structure (as depicted in Fig. 1a). Pressure coefficients are given by the nondimensional ratio:

$$c_p = \frac{\Delta p}{p_{ref}} \tag{1}$$

where Δp is the difference between the pressure measured by the tap on the building surface and the reference static pressure (corresponding to the ambient pressure in the case under investigation [29]). p_{ref} is the reference dynamic pressure, which is measured in the undisturbed upstream flow using a Pitot static tube; it is then reported to the reference height of 10 cm (equivalent to 10 m in full-scale dimensions) by applying the mean wind vertical profile obtained in the absence of the model (Fig. 10a).

Net pressures were determined by subtracting the values of paired pressure taps simultaneously recorded on the outer and inner surfaces of the model. Positive pressures indicate forces directed towards the surface, while positive net pressures indicate downward forces. Peak values were extracted from 1-s averaged time histories using the ensemble average method applied to the maxima (and minima) collected from multiple 10-min intervals in full-scale time.

The pressure tests were conducted at a reference wind speed $\overline{v}_{ref}$ of 10 m/s, resulting in a Reynolds number of $\mathrm{Re} = 3 \times 10^5$. The measurements did not exhibit significant dependency on the Reynolds number, possibly due to the presence of the open edges and the skylight,

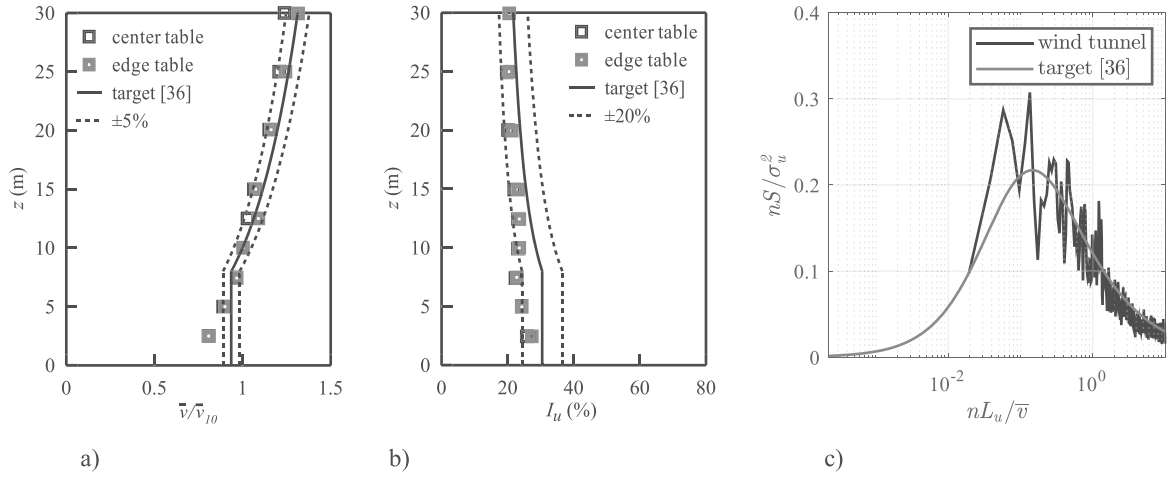

Fig. 10. Profile of the mean wind (a), longitudinal turbulence intensity (b) and corresponding spectrum (c) in the wind tunnel simulation (dashed lines represent the confidence intervals of the target values).

as indicated, e.g., by Refs. [39–41]).

Wind speed at the pedestrian level was investigated at 45° increments, measured with respect to the North (see Fig. 8) in the clockwise wind direction. All measurements were simultaneously sampled at 10 Hz for a total of 60 s.

The employed procedure combines full-scale information with measurements obtained in the wind tunnel. In this regard, real wind speed data $\overline{v}_a$ recorded at the Savona harbour at height $z_a = 12$ m (Section 2.3) are transferred to the site under investigation, at the pedestrian level, through two sequential steps (e.g. Ref. [42]).

First step transfers $\overline{v}_a$ to the campus site at the reference level z_{ref} by the logarithmic law of the wind velocity profile:

$$\overline{v}_{ref}(\alpha) = k_{ref}(\alpha)\overline{v}_a(\alpha), \text{ with } k_{ref}(\alpha) = \frac{\log\left[z_{ref}/z_0(\alpha)\right]}{\log\left[z_a/z_{0,a}(\alpha)\right]} \quad (2)$$

being $z_{0,a}$ and z_0 the roughness coefficients at the anemometer and at the campus site, respectively, z_0 being assumed equal to 0.3 m (Section 3). Based on a specific study at the micro area level around the anemometer [43], $z_{0,a} = 0.09$ m for sea sectors (approximately from 30° to 235° with respect to the north) and $z_{0,a} = 0.15$ m for land sectors (elsewhere).

Second step transforms $\overline{v}_{ref}$ into the velocity $\overline{v}_P$ at each position of interest at the pedestrian level near the roof location, through a transfer coefficient k_P, which depends on the wind direction:

$$\overline{v}_P(\alpha) = k_P(\alpha)\overline{v}_{ref}(\alpha) \quad (3)$$

Transfer coefficients k_P are directly derived from Eq. (3) through the results of wind tunnel tests; $\overline{v}_{ref}$ is measured during the experiments by the "Cobra" probe at the level z_{ref} in an upstream position undisturbed by the built environment; $\overline{v}_P$ is measured by the Kanomax sensors at $z \cong 15$ mm with respect to the ground level (equivalent to 1.5 m in full-scale dimensions).

Subsequently, Equation (3) is employed once again to derive the time history of the 10-min average wind speeds at specific locations of interest near the canopy. This is done using the reference wind speed obtained by applying Equation (2) with real measured data and the k_P coefficients obtained previously from wind tunnel tests. Comfort assessment is therefore investigated in compliance with the Dutch standard NEN8100 [44], based on the probability of exceeding an hourly average wind speed equal to 5 m/s according to the thresholds reported in Table 1. For this purpose, the speed values obtained at the pedestrian level are appropriately adjusted to convert them into 1-h average values following [45].

5. Experimental results

The results of the first trial campaign are presented first. Fig. 11 shows the contour plots of the net mean pressure coefficients measured on the model in its surroundings, mainly driven by the outer surface pressure. At the bottom of the diagrams, an arrow indicates the direction α (Fig. 1a) representing the incoming wind direction. When wind is blowing along the cylindrical axis ($\alpha = 90°$, Fig. 11a), negative pressure coefficients arise on the upwind flat end due to the flow separation from the sharp edge in the outer surface, followed by reattachment and small suction in the remaining region. Wind blowing perpendicular to the cylindrical axis ($\alpha = 0°$, Fig. 11b) gives rise to slight positive pressure on front region of the domed end, while separation bubble and suction arise around the ridge, decreasing to almost constant small negative pressures at the leeward eave, pointing out a large area of flow separation. Skewed wind (α = 150°, Fig. 11c) produces positive pressures on the upwind corner and separation on the following part of the flat upwind edge. Negative pressure on the ridge region is also due to a separation bubble on the outer surface. The presence of the skylight (in addition to the open edges) therefore governs the aerodynamics of this structural shape, fixing the flow separation in the top area of the roofing.

Previous experiments carried out on the model in isolated conditions, detailed in Ref. [29], constitute a benchmark for assessing the role of the actual context with the surroundings. The mean net pressure coefficients for the model in isolation, reported in Fig. 12 for comparison, shows averagely higher pressures and more regular trends, with contour lines almost parallel to the up-wind edge when the wind is blowing parallel and perpendicular to the axis of the cylindrical roof.

Fig. 13 shows the envelope (for all wind directions) of the peak negative and positive net pressure coefficients. The comparison with results for the model in isolation, reported in Fig. 14, highlights the effect of surroundings which breaks down the symmetry (that was apparent for the case in isolation) and mitigates wind pressures, showing maximum positive and negative peak coefficients equal to −5.8 and + 2.8, respectively, to be compared with −6.4 and + 3.6 for the structure in isolation.

The second test campaign specifically aims to conduct flow measurements at selected points near the roof area. With the purpose of evaluating the liveability and comfort of the built area, the primary objective is the evaluation of transfer coefficients $k_P(\alpha)$ of the flow velocity, Eq. (3), which are instrumental in creating wind data databases tailored to specific points of interest. Fig. 15a–h depicts the k_P values for each investigated wind direction (set up 0, no trees) in order to better understand the general wind flow pattern around the canopy roof. These maps highlight the least favorable wind directions at pedestrian level in the different areas. Wind blowing from $\alpha = 0°$, 135°, 180° tends to channel along the pedestrian crossing road (see Fig. 8b), resulting in higher windiness in front of the sports field, especially at taps 1–6. In this area, for $\alpha = 135°$, wind flows almost unobstructed while, for $\alpha = 0°$ (i.e., north direction), it receives some sheltering from the hill and the library building. Wind blowing from $\alpha = 90°$, 225° is channeled through the area between the sports field and the building located to the southeast, creating unfavorable conditions at the taps 9, 10, 11.

Polar diagrams in Fig. 16 supply the transfer coefficients k_P for a selection of taps (taps 1–5) without (setup 0) and with vegetation (setup 1), showing both the shielding and the worsening effect of surrounding buildings and trees for the different directions. However, due to the local wind climate (Fig. 3), windiness at the site is mainly ruled by $\alpha = 315°$. For this direction, k_P is quite large in many positions, highlighting a significant effect of surroundings, which may lead to potential discomfort conditions.

Table 1
Comfort classes [44].

	grade	*activity*		
P(*v* > 5 m/s) (%)		*traversing*	*strolling*	*Sitting*
<2.5	A	good	good	good
2.5–5.0	B	good	good	moderate
5.0–10	C	good	moderate	poor
10–20	D	moderate	poor	poor
>20	E	poor	poor	poor

6. Analysis of the experimental results

The experimental results presented in the previous Section 5 are thoroughly analyzed with specific emphasis on examining the impacts of the surrounding environment. Furthermore, a comprehensive comparison is conducted to evaluate how these results align with literature results and regulatory requirements pertaining to roof pressures. In this regard, it is worth noting that there are no specific Italian or Eurocode regulations that directly address the sustainability of built areas in relation to wind actions.

Fig. 17 reports quantitative comparisons between net pressure coefficients obtained on the model with surroundings (solid lines) and in isolation (dashed lines) along representative lines for the selected directions $\alpha = 90°$ and 0° (Fig. 17a,b) and $\alpha = 150°$ (Fig. 17c and d). The reference line is indicated in each figure; the black arrow indicates the

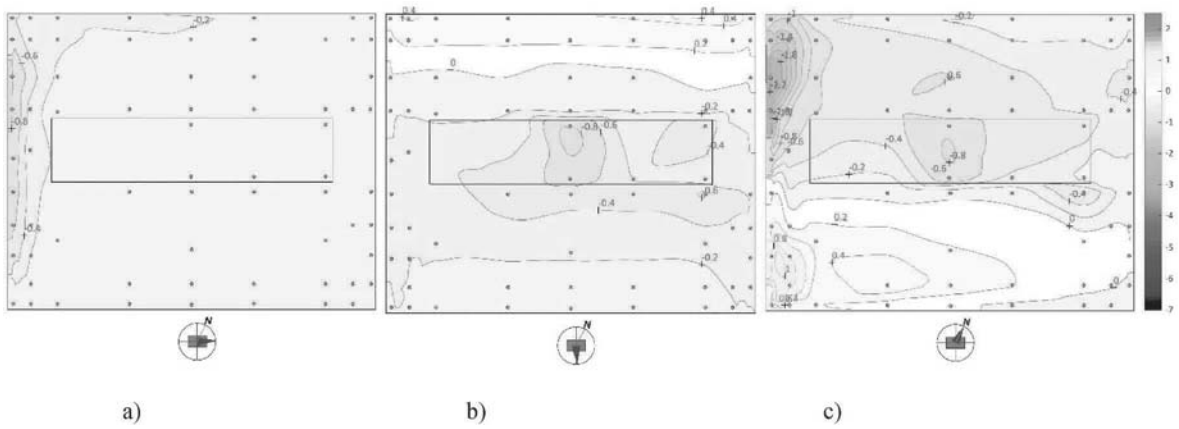

Fig. 11. Mean net pressure coefficients for wind direction parallel to the cylindrical axis, $\alpha = 90°$ (a), perpendicular, $\alpha = 0°$ (b), skewed, $\alpha = 150°$ (c) for the roofing structure with surroundings.

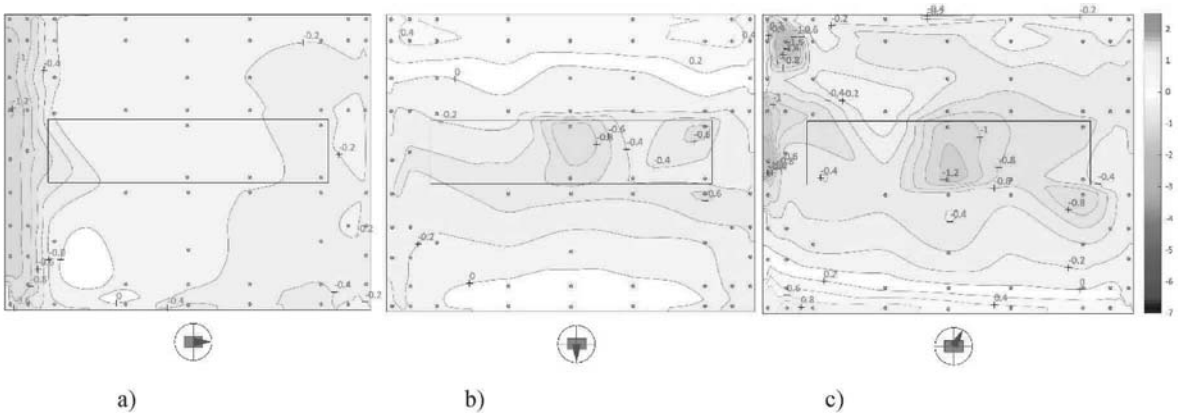

Fig. 12. Mean net pressure coefficients for wind direction parallel to the cylindrical axis, $\alpha = 90°$ (a), perpendicular, $\alpha = 0°$ (b), skewed, $\alpha = 150°$ (c) for the roofing structure in isolation.

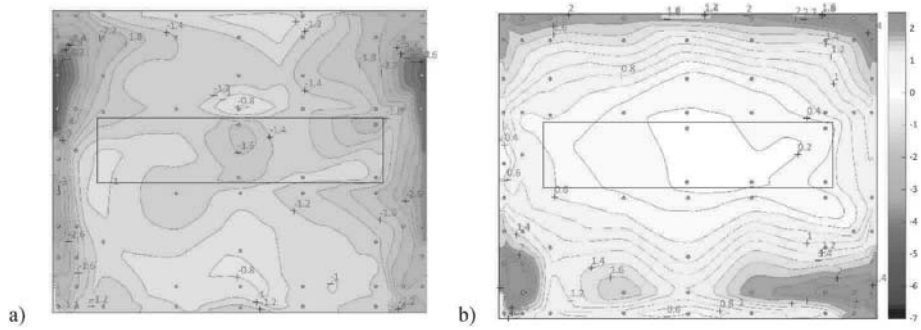

Fig. 13. Negative (a) and positive (b) peak envelope of net pressure coefficients for the model with surroundings.

wind direction. The upper and lower lines represent the positive and negative peak values; the inner line represents the mean values. The diagrams show an average mitigation of pressures for the model in surroundings. However, for skewed wind (Fig. 17c and d), in the area closed to the flat edge, where separation bubbles occur, the model with its surroundings undergoes huge local increase of pressures (both mean values and peaks) with respect to the model in isolation. This fact is especially relevant for local load assessment rather than global loading, which instead is estimated through the mean values. Fig. 18 reports the envelopes of the negative (a) and positive peak net coefficients (b) for the model with surroundings (solid line) and in isolation (dashed line) along equally spaced lines. The comparison reveals that the highest loads still occur for the model in isolation although, in certain alignments, the surroundings can contribute to an increase in wind-induced pressures.

Detailed experiments on free standing vaulted canopies are quite few. Cook [46] proposed a qualitative framework that was drawn from an arch with a rise to span ratio equal to 0.25 and 0.125; flow separation occurs when the wind is perpendicular to the axis of the cylinder, producing positive pressure on the front of the canopy, suction on the crest followed by pressure recovery. Natalini et al. [47] detailed the outcomes of an experimental campaign on open arched canopies exploring mean pressure coefficients for different geometries and dimensions; the f/B ratio was 0.2. Uematsu and Yamamura [48] tested a number of open

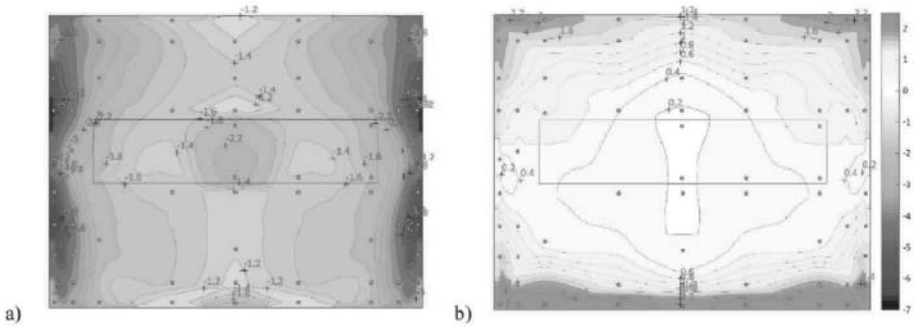

Fig. 14. Negative (a) and positive (b) peak envelope of net pressure coefficients for the model in isolation.

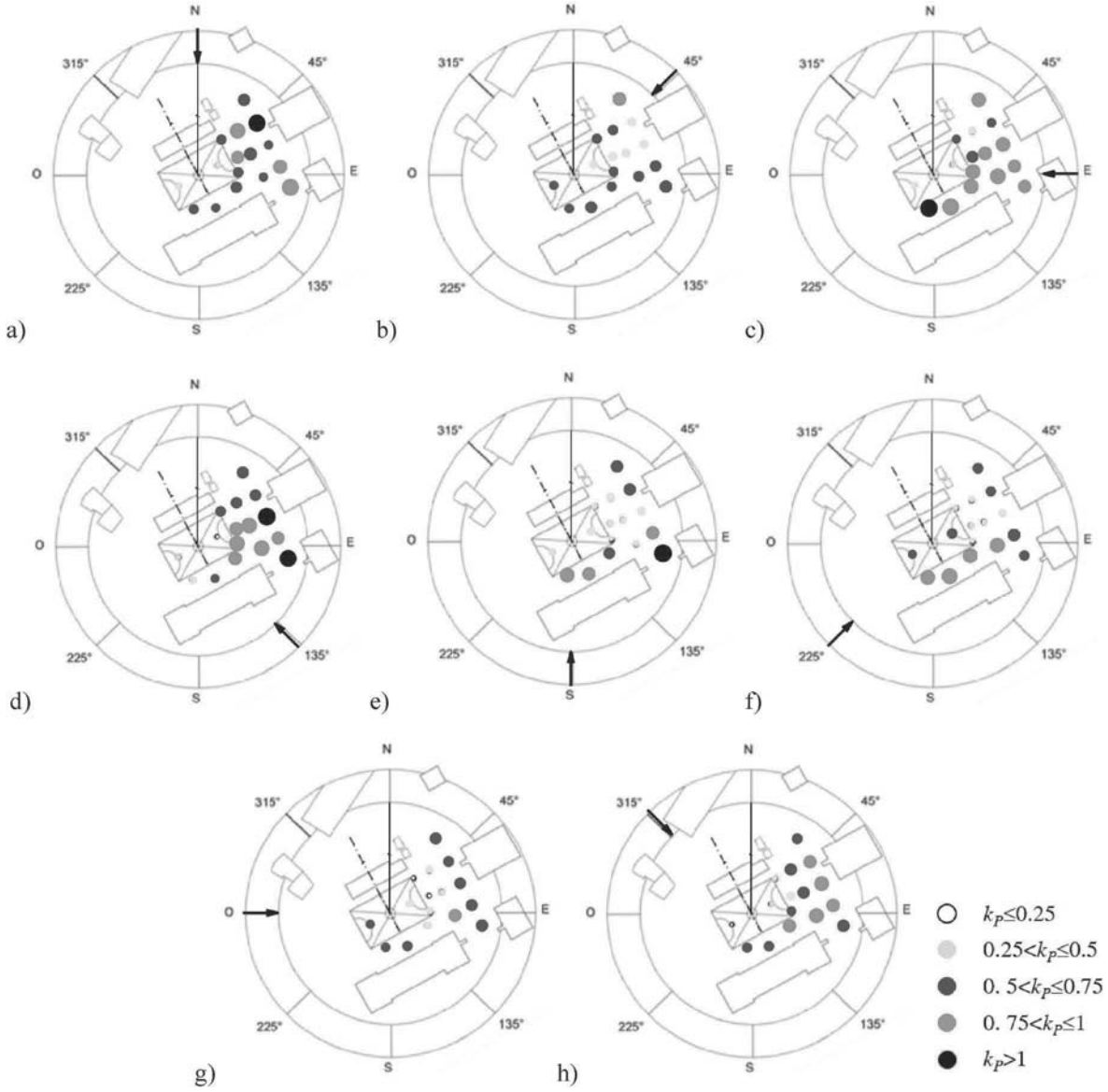

Fig. 15. Maps of the transfer coefficients k_P for set up 0 (without trees) for the wind directions $\alpha = 0°, \ldots 315°$, in steps of 45° (a, b, … h), indicated by the black arrows (the size of each dot is proportional to its value).

cylindrical roof models proposing mean pressure coefficients for design as a function of the rise-to-span ratio. In a recent paper, Ding and Uematsu [49] provide some information on peak values too, supplying contour maps for selected wind directions for the only case $f/B = 0.1$.

Fig. 19 reports a comparison with literature experiments along a selected line of the canopy, perpendicular to the cylindrical axis, when wind speed is blowing parallel to this line. The results presented for the case being investigated are derived from Fig. 17b. In detail, Fig. 19a reports the mean net coefficients obtained in the experiment, together with values from Refs. [47,48] at $f/B = 0.1, 0.2, 0.3$. Fig. 19b reports the

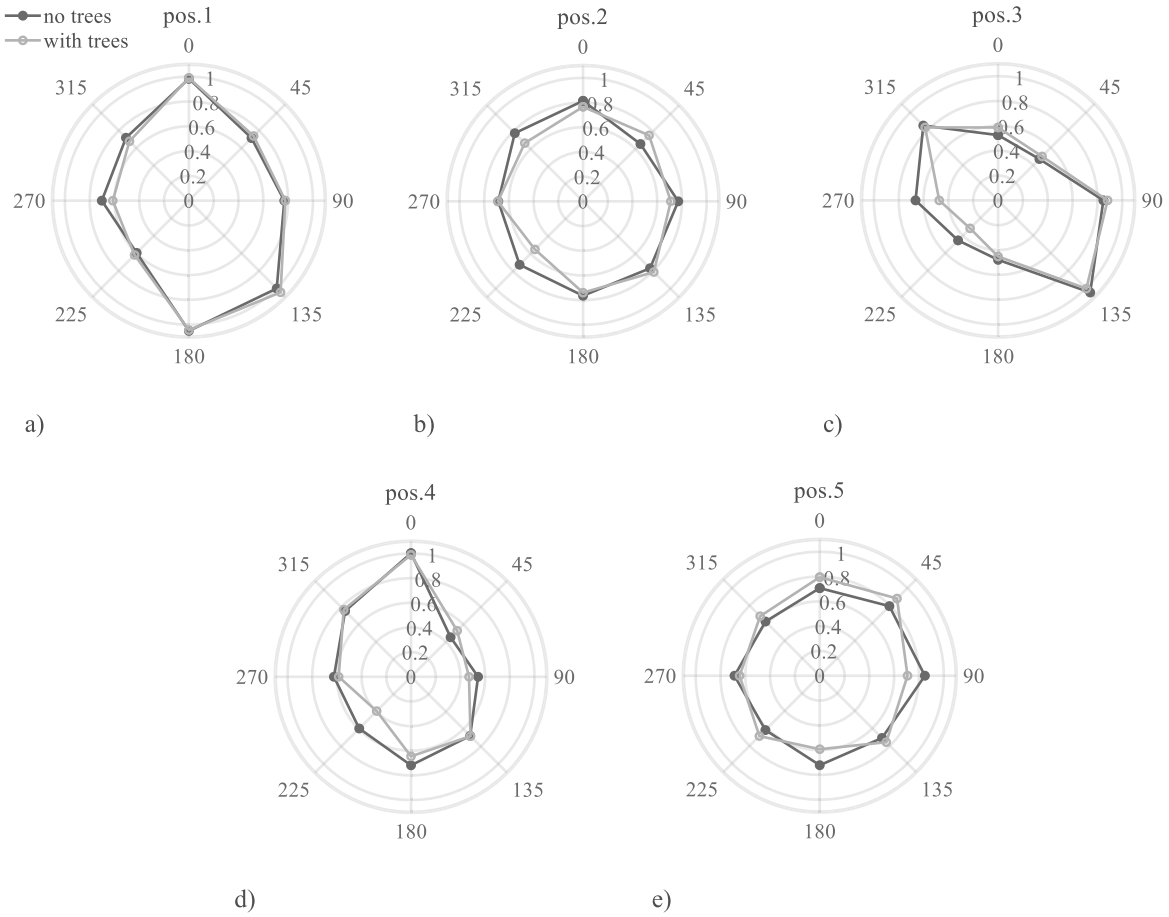

Fig. 16. Transfer coefficients k_P for setup 0 (without trees) and 1 (with trees) for positions 1–5 (a–e).

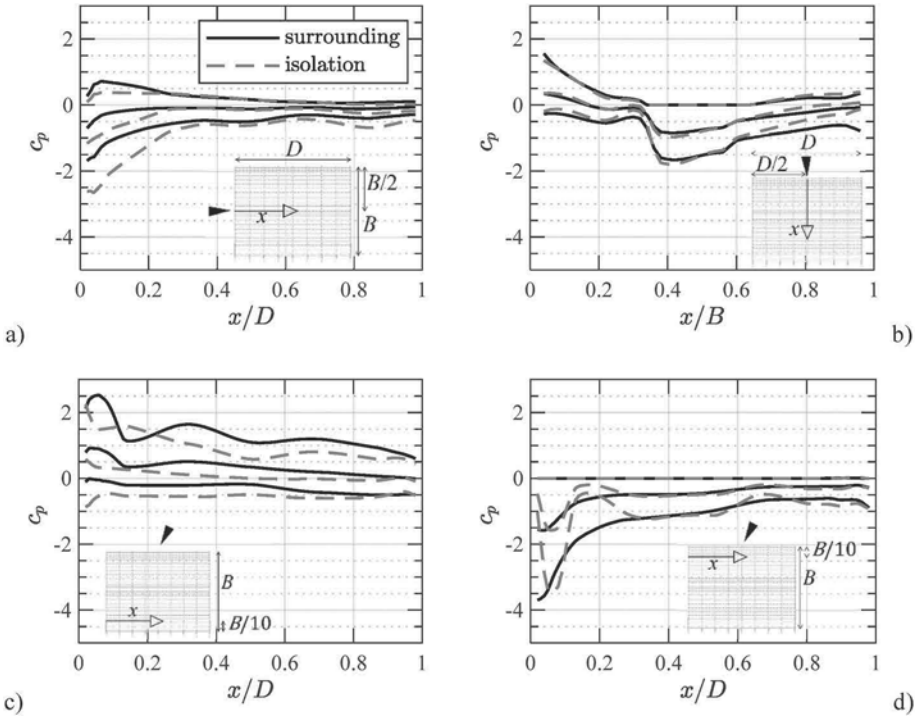

Fig. 17. Comparison between net pressure coefficients along a line for the model with surroundings (solid line) and in isolation (dashed line). The filled black arrow indicates the wind direction. The upper and lower lines represent the positive and negative peak values; the inner line represents the mean coefficients for $\alpha = 90^\circ$ (a), 0° (b), 30° (c, d).

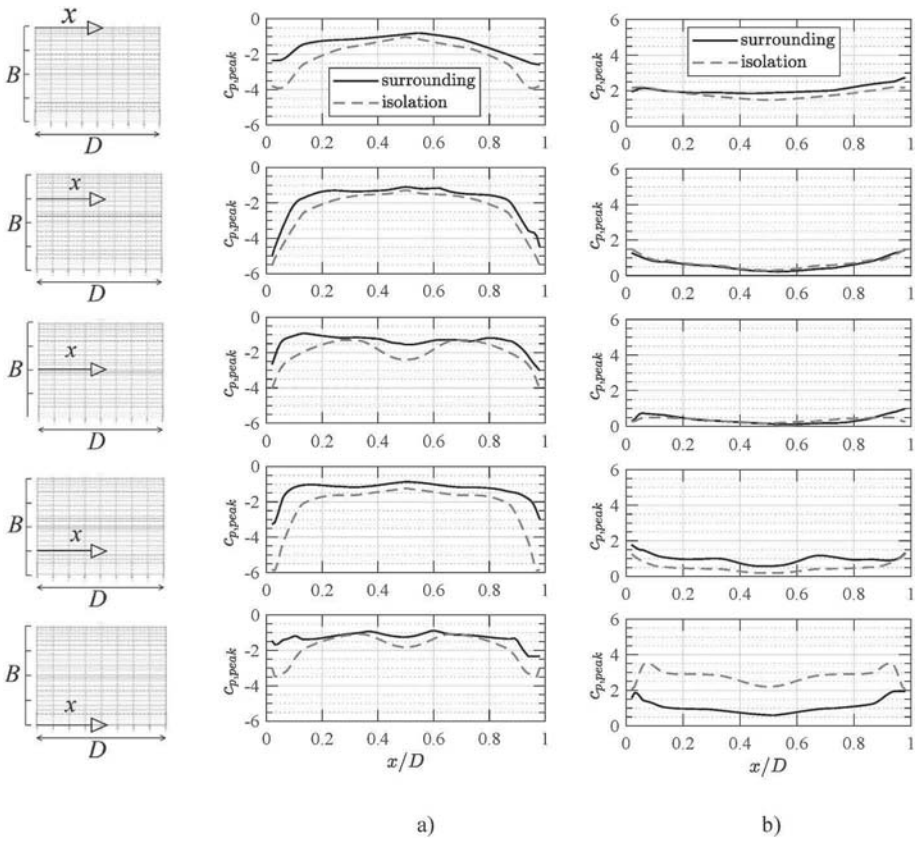

Fig. 18. Negative (a) and positive (b) peak envelope of net pressure coefficients for the model with surroundings (solid lines) and in isolation (dashed lines).

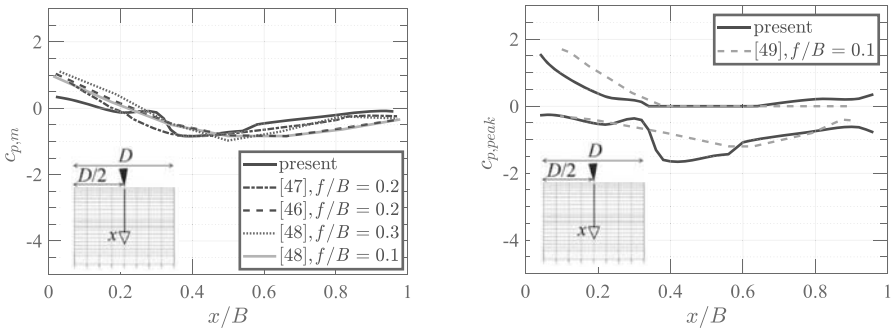

Fig. 19. Mean (a) and peak net pressure coefficients (b) along a central line for the wind direction perpendicular to the cylindrical axis, $\alpha = 0°$: comparison between the present experimentation and literature results.

net positive and negative peak values along the same line, compared with values from Ref. [49], obtained at $f/B = 0.1$. The diagrams show a qualitative agreement together with discrepancies, due to differences in geometry, roof level with respect to the ground (the canopy investigated in the present study is much closer to the ground than the other models), as well as uncertainties in the definition of rise-to-span ratio for the present experiment. In particular, the influence of surroundings and of the small building on which the roof rests (in the upwind side) significantly modify the pressure field on the upwind region. Large discrepancies occur in Fig. 19a and b at the leading edge of the canopy, where the investigated model experiences a decrease in the pressure field compared to the reference cases. Results reported in Ref. [43] show that the presence of the surrounding and of the small building are almost entirely responsible of such discrepancies. At the opposite side, in the leeward area, discrepancies could be attributed to the canopy shape. In Fig. 19a, the differences from the dotted line, supplied by Ref. [48] for $f/B = 0.2$, are reduced considering $f/B = 0.3$ (dotted line). Large discrepancies in terms of negative peak pressures around the ridge reported by the present experiment (for $0.35 < x/B < 0.55$) can be related to the presence of the skylight that rules flow separation. It is also to be observed that the comparison in terms of peak pressures (Fig. 19b) is purely indicative as the two cases have different f/B ratios.

Codes and standards for wind actions do not supply specific pressure coefficients for vaulted open canopies, nor can they consider the influence of the surrounding environment and vegetation. In this case, as an alternative to performing specific studies, pressure evaluation can refer to either free standing pitched roofs or vaulted roof buildings. The use of pressure coefficients for vaulted roof buildings may be unsafe, as does not consider the contribution of internal pressures. Reference to open pitched roof can be done by using coefficients for flat roof in isolation when the wind is blowing parallel to the cylindrical axis. When the wind is blowing perpendicular to the cylindrical axis, an open duo-pitched

roof can be considered, since the presence of the skylight can have an aerodynamic effect similar to that of the ridge of a gabled roof. Assuming a pitch angle $\varphi = 20^\circ$ (corresponding to the dashed line in Fig. 1b), Fig. 20 shows a comparison between the values deriving from the wind tunnel experiments of the model with its surroundings (solid line) and values provided by the European Code EN 1991-1-4 [50]. Fig. 20a,c reports the mean value of the net pressure coefficients along a central line for wind parallel ($\alpha = 90^\circ$) and perpendicular to the cylindrical axis ($\alpha = 0^\circ$). Fig. 20b,d reports the positive and negative peak values for the same alignments. Solid lines supply the values obtained from the experiments, while dotted lines report the values derived from the European Code. The diagrams show a satisfactory agreement, notwithstanding the obvious (and in some positions substantial) overestimation that can be expected from the Code. At the same time, this overall overestimation does not protect the construction from local criticalities, because the flow separation near the edges creates high-pressure peaks, as noted in the discussion of Fig. 17. Therefore, comprehensive wind tunnel analyses allow optimizing the design, reducing material usage and carbon footprint, and enhance safety, by addressing peak load scenarios that may arise from high wind speeds approaching design values.

Shifting our focus on evaluating how the new construction impacts the area's liveability, Fig. 21 supplies the comfort categories (based on Table 1) for the two configurations in setup 0 and 1, showing definitely good comfort inside the covered field (positions 12–16) and some criticisms elsewhere. Comparison between the diagrams for the two setups highlights the general beneficial effect of vegetation with exception of taps 4 and 5, where it is responsible for accelerating the flow for some wind directions (as occurred in Ref. [51]). The presence of trees improves liveability of the positions immediately around the sports field, where people may stand watching sports competitions (positions 6–16), leading them to moderate and good comfort category for any possible activity. At the most, some moderate comfort is highlighted for static activities (such as sitting) in front of the field, positions 6, 7, 8. Notwithstanding the presence of trees, moderate comfort conditions persist in positions 1–5, especially in taps 3 and 4 for strolling, turning into poor comfort for static activities. These pressure taps are positioned along the pedestrian street, which is a frequently traversed route leading to classrooms, offices, restaurants, and key destinations of the university campus. Considering that people generally move at a brisk pace in these areas, the resulting comfort level can be classified as moderate.

The dynamic presence of people is a crucial factor to consider when assessing the usability of a university campus area, which experiences significant fluctuations throughout the day and varies across different months of the year. Therefore, it is essential to re-evaluate pedestrian comfort from a different perspective that takes into account the average variation of wind speed throughout the day and the predominant pedestrian activities during various time intervals. Fig. 22 reports the hourly variation of the average wind speed, transferred to the site at the reference level, for each investigated wind sector. Each figure reports the results for two opposite wind directions along the same line, specifically 0°–180°, 45°–225°, 90°–270°, 135°–315°, along with the corresponding percentage of occurrence in the specified directions. In addition to the significantly higher average speeds during the day in land sectors (black lines), already highlighted in Fig. 5a, there is an opposite trend observed in sea sectors (grey lines), where wind speed values are lower during the central hours of the day. Direction $\alpha = 45^\circ$, which is close to the coastal line acting as a boundary between the sea and the land areas, deviates from this trend, while it is very clear for $\alpha = 135^\circ$, where wind speed is considerably higher from late afternoon to early morning. Such phenomenon is reflected in the hourly exceedance probability shown in Fig. 23 for the model with surroundings and actual vegetation (setup 1) for positions 1–5, which have highlighted the major criticisms for pedestrian comfort. The diagrams also report results related to setup 0, without trees, and further results with the presence of more trees (setup 2). In addition to emphasizing the significance of vegetation for enhancing the liveability of open-air spaces, these Figures demonstrate that the comfort level varies significantly throughout the day. As a result, certain positions that were initially deemed uncomfortable can actually be considered satisfactory during hours with a higher pedestrian presence (e.g., positions 3 and 4). On the contrary, some other positions, that were considered to be comfortable on average, actually exhibit potential criticalities (e.g., position 1) during operating hours. Windiness in position 1 is especially ruled by wind blowing from the North and the South, as well as by the frequent wind coming from $\alpha = 315^\circ$. Considering the actual presence of trees (setup 1), it averagely falls in comfort class C (good comfort for traversing, moderate and poor for strolling and sitting). However,

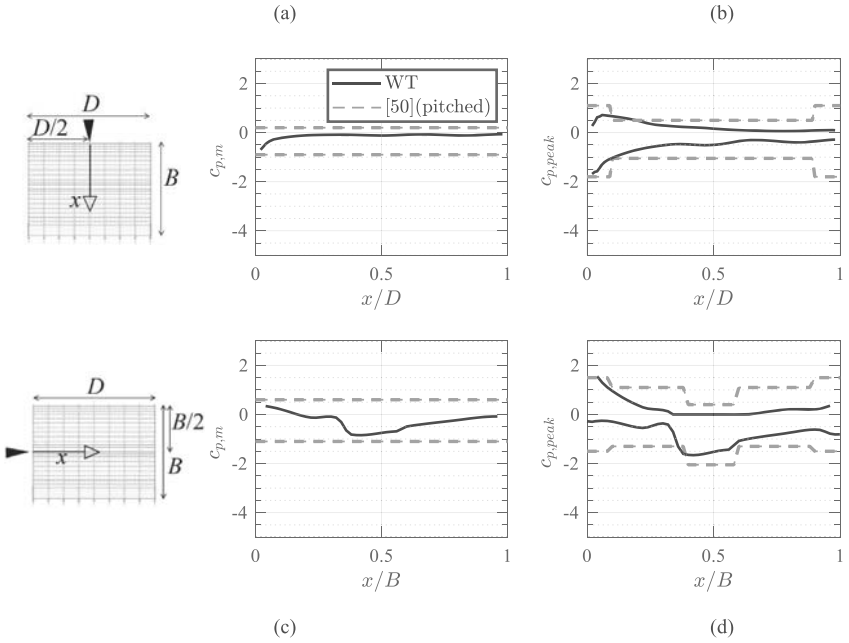

Fig. 20. Pressure net coefficient profiles for the model with surroundings (solid line) and provisions by EN 1991-1-4 [50] (dashed lines); mean (a) and maximum positive and negative coefficients (b) for $\alpha = 90^\circ$ and for $\alpha = 180^\circ$ (c, d).

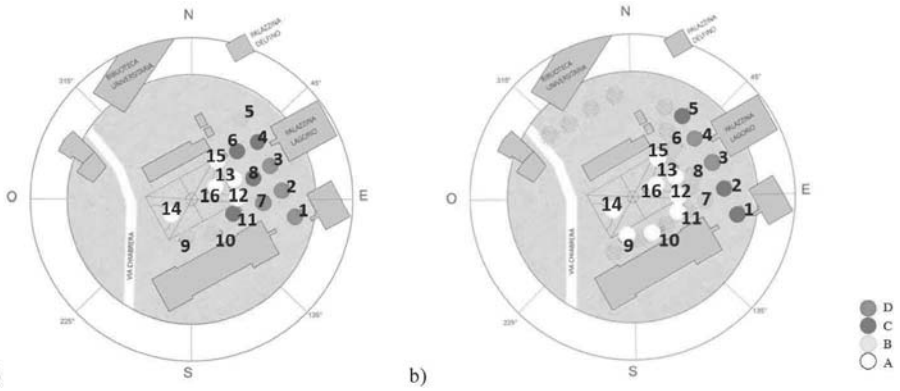

Fig. 21. Comfort categories for setup 0 (without trees, a) and 1 (with trees, b).

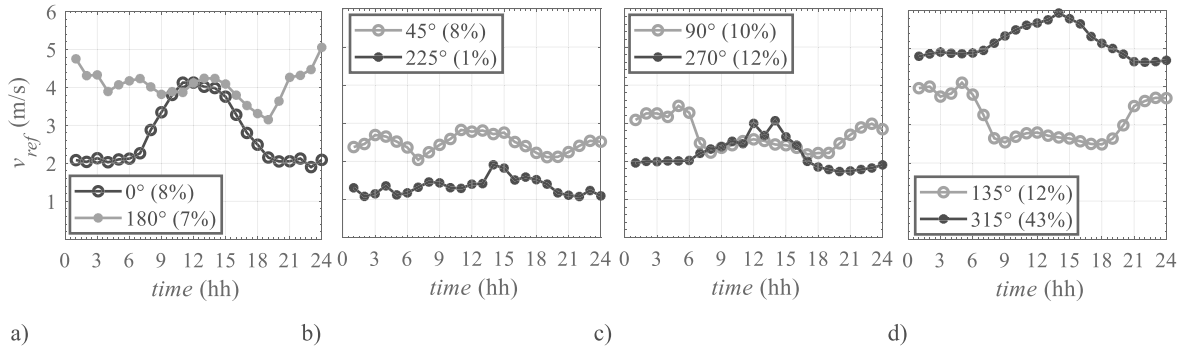

Fig. 22. Hourly reference wind speed for different wind sectors for sectors 0°–180° (a), 45°–125° (b), 90°–270° (c), 135°–315° (d) (grey lines represent sea sectors, black lines land sectors).

coherently with what highlighted for the prevalent sector, windiness is especially high in the central hours of the day. Consequently, this position falls in comfort class D (moderate comfort for traversing, poor for strolling and sitting) during the noon time, when students and people living the campus usually walk to reach the cafeteria or take a break during the warmest hours, especially when the climate is milder. On the other hand, the presence of dense trees constitutes a barrier capable of mitigating the windiness of the site, bringing to more comfortable conditions. Besides wind direction $\alpha = 315°$, windiness in position 3 is also ruled by $\alpha = 90°$ and 135°, which produce higher wind speed at night. Even if it averagely falls in class D, the strongest wind conditions occur at night, when the campus is empty, and early in the morning, when people walk quickly and are not disturbed by a moderate breeze. Windiness is mitigated at noon and especially in the afternoon. A similar situation is observed in position 4. Finally, it is noted that, in positions 4 and 5, the presence of trees does not provide any mitigation and even worsen the pedestrian comfort.

7. Conclusions and perspectives

Using accurate wind speed recordings and wind tunnel experiments, this paper discusses the effect of urban environment and vegetation on a new sports field in a university campus, addressing its sustainability in terms of structural optimization, well-being and safety related to wind actions and effects on the built-up area.

The key aspects of interest in this work are the following.

- The roofing structure analyzed is commonly found in social areas such as sports centres and university campuses, but it is not currently regulated by wind codes and guidelines. The incorporation of surroundings in the experimental tests, including other buildings, topography and vegetation, adds substantial value to the study.
- The aerodynamics behavior of the roofing structure is strongly influenced by the presence of the skylight at its top, which fixes the flow separation point. The skylight also seems to be accountable for the main significant discrepancies compared to similar roofing structures in the literature. Specifically, large negative peaks of net pressure were observed close to the skylight area in contrast to the sole case documented in the literature that provides data on peak values.
- The wind pressure coefficients of the roofing structure within its specific environment, in terms of net average and peak values, are compared with the values obtained for the model in isolation. The findings reveal that the presence of the environment generally mitigates wind-induced pressures, although in certain localized cases it can lead to pressure increase. The values derived from codes and standards, typically used in the absence of specific information, appear excessively conservative. Consequently, they result in an overuse of structural materials without adequately indicating the actual local criticalities associated with the specific structural shape.
- The presence of vegetation contributes to a general reduction in windiness, resulting in enhanced comfort for area users. Additional improvements can be achieved by introducing small new trees alongside existing ones, representing potential future scenarios. However, in certain locations, the wake effects caused by trees can lead to localized increases in wind speed at pedestrian level. These findings, along with the pressure results, highlight the importance of establishing guidelines regarding the optimal tree species for interventions aimed at improving comfort and mitigating wind effects. Furthermore, determining the optimal arrangement of trees is crucial

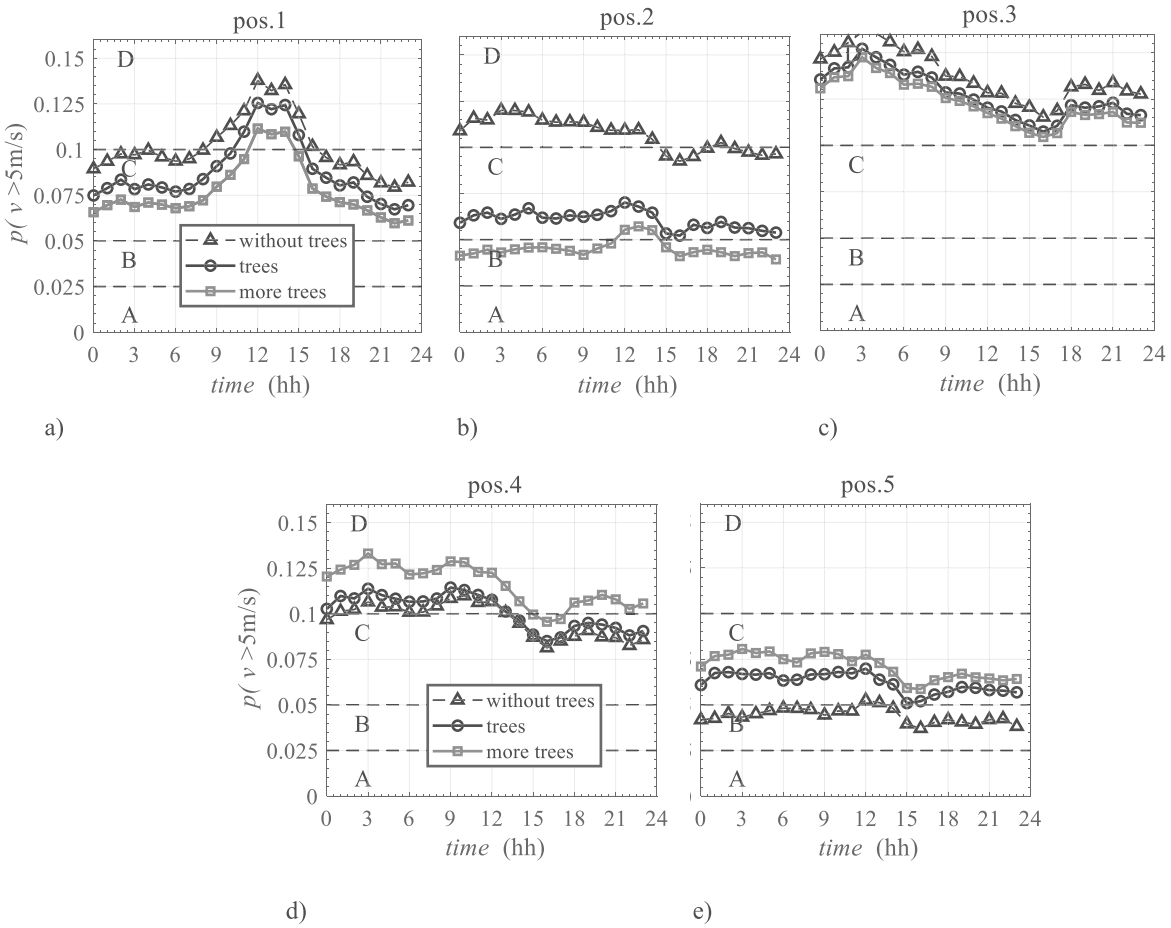

Fig. 23. Hourly exceedance probability at positions 1–5 (a–e).

to effectively enhance pedestrian comfort and sustainability in general.

- A comprehensive analysis of comfort classes, considering both the intended use of the area and the specific times of the day, reveals potential variations. Considering the dynamic nature of campus activities and varying pedestrian presence throughout the day, the innovative approach of assigning comfort classes at different times proves to be relevant. This procedure leads to a different scenario where certain locations, previously characterized by moderate discomfort, experience satisfactory pedestrian comfort. This is due to the strongest winds occurring when the area is less populated or when individuals quickly transit to classrooms and offices. Conversely, other positions may fall within the moderate discomfort threshold on average but exceed it when people take afternoon breaks or attend sporting events. These findings emphasize the need to evaluate the area liveability considering the daily activities at the specific site in question.

It is important to note that, to the best of the authors' knowledge, there is currently no standardized representation in the literature for reproducing vegetation at the scale of a wind tunnel, including the types of trees and their arrangement. This aspect holds significant importance since the effects of real trees may not be entirely replicable at a scaled-down level in terms of their impact on the roof and overall comfort. Therefore, the results derived from the influence of vegetation are necessarily approximated, and it is hoped that future standardization efforts in utilizing these procedures will enhance reproducibility and facilitate comparisons among different investigated cases.

Finally, it is noted that the completion of this study should also include an experimental analysis of the dispersion of pollutants, which can somehow benefit from higher land breezes [52]. Unfortunately, at present, adequate measures for this purpose are not available at the Savona University campus. It is hoped that new appropriate measuring units will be installed to proceed in this direction. Furthermore, an optimal study of the position of the vegetation could also have considerable importance for the study of heat waves, for which the experimental part should be accompanied by computational studies (e.g. Ref. [53]).

CRediT authorship contribution statement

Luisa Pagnini: Writing – original draft, Software, Methodology, Investigation, Formal analysis, Data curation, Conceptualization. **Federico Delfino:** Funding acquisition, Conceptualization. **Giuseppe Piccardo:** Writing – review & editing, Methodology, Funding acquisition, Formal analysis, Conceptualization. **Maria Pia Repetto:** Writing – review & editing, Methodology, Conceptualization.

Data availability

Data will be made available on request.

Acknowledgments

This study was carried out within the RETURN Extended Partnership and received funding from the European Union Next-Generation EU (National Recovery and Resilience Plan – NRRP, Mission 4, Component 2, Investment 1.3 – D.D. 1243 2/8/2022, PE0000005).

References

[1] Y. Cang, L. Yang, Z. Luo, N. Zhang, Prediction of embodied carbon emissions from residential buildings with different structural forms, Sustain. Cities Soc. 54 (2020), 101946.

[2] Y. Sun, S. Hao, X. Long, A study on the measurement and influencing factors of carbon emissions in China's construction sector, Build. Environ. 229 (2023), 109912.

[3] A.-A. Kafy, A.-A. Faisal, A. Al Rakib, M.A. Fattah, Z.A. Rahaman, G.S. Sattar, Impact of vegetation cover loss on surface temperature and carbon emission in a fastest-growing city, Cumilla, Bangladesh, Build. Environ. 208 (2022), 108573.

[4] Z.A. Rahaman, A.-A. Kafy, M. Saha, A.-A. Faisal, A. Al Rakib, Assessing the impacts of vegetation cover loss on surface temperature, urban heat island and carbon emission in Penang city, Malaysia, Build. Environ. 222 (2022), 109335.

[5] Cities100, 100 City Projects Making the Case for Climate Action, 2019. https://www.c40knowledgehub.org.

[6] T. O'Mahony, Toward sustainable wellbeing: advances in contemporary concepts, Front. Sustain. 3 (2022), 807984.

[7] A. Elshaer, A. Gairola, K. Adamek, G. Bitsuamlak, Variations in wind load on tall buildings due to urban development, Sustain. Cities Soc. 34 (2017) 264–277.

[8] K.T. Tse, X. Zhang, A.U. Weerasuriya, C.M. Mak, J. Niu, Adopting 'lift-up' building design to improve the surrounding pedestrian-level wind environment, Build. Environ. 117 (2017) 154–165.

[9] N. Metje, M. Sterling, C.J. Baker, Pedestrian comfort using clothing values and body temperatures, J. Wind Eng. Ind. Aerod. 96 (4) (2008) 412–435.

[10] A. Norouziasas, P. Pilehchi Ha, M. Ahmadi, H. Bahadur Rijal, Evaluation of urban form influence on pedestrians' wind comfort, Build. Environ. 224 (2022), 109522.

[11] E. Willemsen, J.A. Wisse, Design for wind comfort in The Netherlands: procedures, criteria and open research issues, J. Wind Eng. Ind. Aerod. 95 (9–11) (2007) 1541–1550.

[12] H. Mittal, A. Sharma, A. Gairola, A review on the study of urban wind at the pedestrian level around buildings, J. Build. Eng. 18 (2018) 154–163.

[13] City of London, Wind Microclimate Guidelines for Developments in the City of London, 2019. https://www.cityoflondon.gov.uk.

[14] W.D. Janssen, B. Blocken, T. van Hooff, Pedestrian wind comfort around buildings: comparison of wind comfort criteria based on whole-flow field data for a complex case study, Build. Environ. 59 (2013) 547–562.

[15] W. Wang, H. Chen, L. Wang, S. Wang, Integrating multiple models into computational fluid dynamics for fine three-dimensional simulation of urban waterfront wind environments: a case study in Hangzhou, China, Sustain. Cities Soc. 25 (2022), 104088.

[16] S. Zhang, K.C.S. Kwok, B. Wang, A CFD study of wind assessment in urban topology with complex wind flow, Sustain. Cities Soc. 11 (2021), 103006.

[17] B. Blocken, T. Stathopoulos, J.P.A.J. van Beeck, Pedestrian-level wind conditions around buildings: review of wind-tunnel and CFD techniques and their accuracy for wind comfort assessment, Build, Environ. Times 100 (2016) 50–81.

[18] UK Wind Engineering Society, A Position Paper on Experimental and Computational Methods in Wind Engineering, 2022. https://www.windengineering.org.uk.

[19] K. Adamek, N. Vasan, A. Elshaer, E. English, G. Bitsuamlak, Pedestrian level wind assessment through city development: a study of the financial district in Toronto, Sustain. Cities Soc. 35 (2017) 178–190.

[20] A. Ricci, M. Guasco, F. Caboni, M. Orlanno, A. Giachetta, M.P. Repetto, Impact of surrounding environments and vegetation on wind comfort assessment of a new tower with vertical green park, Build. Environ. 207 (2022), 108409.

[21] S. Teshnehdel, H. Akbari, E. Di Giuseppe, R.D. Brown, Effect of tree cover and tree species on microclimate and pedestrian comfort in a residential district in Iran, Build, Environ. Times 178 (2020), 106899.

[22] X. He, W. Gao, R. Wang, Impact of urban morphology on the microclimate around elementary schools: a case study from Japan, Build. Environ. 206 (2021), 108383.

[23] T. Zhang, B. Hong, X. Su, Y. Li, L. Song, Effects of tree seasonal characteristics on thermal-visual perception and thermal comfort, Build. Environ. 212 (2022), 108793.

[24] G. Kang, J.-J. Kim, D.-J. Kim, W. Choi, S.-J. Park, Development of a computational fluid dynamics model with tree drag parameterizations: application to pedestrian wind comfort in an urban area, Build. Environ. 124 (2017) 209–218.

[25] G. Kang, J.-J. Kim, W. Choi, Computational fluid dynamics simulation of tree effects on pedestrian wind comfort in an urban area, Sustain. Cities Soc. 56 (2020), 102086.

[26] F. Barbano, S. Di Sabatino, R. Stoll, E.R. Pardyjak, A numerical study of the impact of vegetation on mean and turbulence fields in a European-city neighborhood, Build. Environ. 186 (2020), 107293.

[27] S. Zhu, F. Causone, N. Gao, Y. Ye, X. Jin, X. Zhou, X. Shi, Numerical simulation to assess the impact of urban green infrastructure on building energy use: a review, Build. Environ. 228 (2023), 109832.

[28] D.H.S. Duarte, P. Shinzato, C.S. Gusson, C.A. Alves, The impact of vegetation on urban microclimate to counterbalance built density in a subtropical changing climate, Urban Clim. 14 (2015) 224–239.

[29] L. Pagnini, S. Torre, A. Freda, G. Piccardo, Wind pressure measurements on a vaulted canopy roof, J. Wind Eng. Ind. Aerod. 223 (2022), 104934.

[30] S. Bracco, F. Delfino, P. Laiolo, A. Morini, Planning & open-air demonstrating smart city sustainable districts, Sustainability 10 (2018) 4636.

[31] M. de Simón-Martín, S. Bracco, G. Piazza, L.C. Pagnini, A. González-Martínez, F. Delfino, Application to real case studies, in: Levelized Cost of Energy in Sustainable Energy Communities, SpringerBriefs in Applied Sciences and Technology, Springer, Cham, 2022, pp. 77–120, https://doi.org/10.1007/978-3-030-95932-6_4.

[32] T.S. Chapin, Sports facilities as urban redevelopment catalysts, J. Am. Plann. Assoc. 70 (2) (2004) 193–209.

[33] G. Solari, M.P. Repetto, M. Burlando, P. De Gaetano, M. Pizzo, M. Tizzi, M. Parodi, The wind forecast for safety management of port areas, J. Wind Eng. Ind. Aerod. 104–106 (2012) 266–277.

[34] S.A. Akdağ, H.S. Bagiorgas, G. Mihalakakou, Use of two-component Weibull mixtures in the analysis of wind speed in the Eastern Mediterranean, Appl, Energy 87 (2010) 2566–2573.

[35] L. Pagnini, G. Piccardo, M.P. Repetto, Full scale behavior of a small size vertical axis wind turbine, Renew. Energy 127 (2018) 41–55.

[36] CNR, Guide for the Assessment of Wind Actions and Effects on Structures – CNR-DT 207/2008, National Research Council of Italy, Rome, 2010.

[37] A. Jafari, F. Ghanadi, M.J. Emes, M. Arjomandi, B.S. Cazzolato, Measurement of unsteady wind loads in a wind tunnel: scaling of turbulence spectra, J. Wind Eng. Ind. Aerod. 193 (2019), 103955.

[38] H.W. Tieleman, Wind tunnel simulation of wind loading on low-rise structures: a review, J. Wind Eng. Ind. Aerod. 91 (2003) 1627–1649.

[39] J.D. Holmes, Determination of Wind Loads for an Arch Roof, Civil Engineering Transactions, Institution of Engineers Australia, 1984.

[40] Y. Qiu, Y. Sun, Y. Wu, Y. Tamura, Modeling the mean wind loads on cylindrical roofs with consideration of the Reynolds number effect in uniform flow with low turbulence, J. Wind Eng. Ind. Aerod. 129 (2014) 11–21.

[41] C.W. Letchford, P.P. Sarkar, Mean and fluctuating wind loads on rough and smooth parabolic domes, J. Wind Eng. Ind. Aerod. 88 (2000) 101–117.

[42] M.P. Repetto, M. Burlando, G. Solari, P. De Gaetano, M. Pizzo, Integrated tools for improving the resilience of seaports under extreme wind events, Sustain. Cities Soc. 32 (2017) 277–294.

[43] L.C. Pagnini, M. Burlando, M.P. Repetto, Experimental power curve of small-size wind turbines in turbulent urban environment, Appl. Energy 154 (2015) 112–121.

[44] NEN, Netherlands Normalisation Institute, Wind Comfort and Wind Danger in the Built Environment, NEN 8100, 2006. March (in Dutch).

[45] ASCE. Aerodynamics Committee, Outdoor Human Comfort and its Assessment, State of the Art Report, Task Committee on Outdoor Human Comfort, Boston, VA, USA, 2003.

[46] N.J. Cook, The Designer's Guide to Wind Loading of Building Structures - Part2: Static Structures, Building Research Establishment, London, 1990.

[47] M.B. Natalini, C. Morel, B. Natalini, Mean loads on vaulted canopy roofs, J. Wind Eng. Ind. Aerod. 119 (2013) 102–113.

[48] Y. Uematsu, R. Yamamura, Wind loads for designing the main wind-force resisting systems of cylindrical free-standing canopy roofs, Technical Transactions 7 (2019) (2019) 125–144.

[49] W. Ding, Y. Uematsu, Discussion of design wind loads on a vaulted free roof, Wind 2 (2022) 479–494.

[50] EN 1991-1-4, Eurocode 1: Actions on Structures – Part 1.4: General Actions – Wind Actions, CEN, European Committee for Standardization, Brussels, Belgium, 2005.

[51] Z. Jian, L. Bo, W. Mingyue, Study on windbreak performance of tree canopy by numerical simulation method, J. Comput. Multiph. Flows 10 (4) (2018) 259–265.

[52] E. Keshavarzian, K.C.S. Kwok, K. Dong, K. Chauhan, Y. Zhang, An experimental Investigation of stagnant air pollution dispersion around a building in a turbulent flow, Build. Environ. 224 (2022), 109564.

[53] Y. Toparlar, B. Blocken, P. Vos, H. Montazeri, H.J.P. Timmermans, CFD simulation and validation of urban microclimate: a case study for Bergpolder Zuid, Rotterdam, Build, Environ. Times 83 (2015) 79–90.